The cumulative data in this study showed a strong correlation between L/B ratios calculated on attenuation-corrected and uncorrected images (Fig. 3). However, there was no correlation between SUR values calculated on both types of images. This is probably due to the fact that the background activity, an important variable in these calculations, is not considered in SUR calculations. Moreover, absolute counts are required for the original definition of SUR. For the same reasons, SUR and L/B values calculated on uncorrected images also did not show a significant correlation (Fig. 5). This indicates that the L/B ratio is the only index that can be used for semiquantitative evaluation of uncorrected images.

Our results confirmed that the attenuation correction required for quantitative studies is not essential for qualitative imaging in PET oncological studies. Thus, qualitative or semiquantitative evaluation of nonattenuation-corrected images seems to be sufficient for the effective use of whole-body FDG PET scans in diagnosing malignant and benign lesions. However, recognition of the artifactual enhancement of body surface and certain organs such as the liver is essential.

CONCLUSION

We have demonstrated that attenuation-uncorrected images provide not only clinically useful but also as much quantitative information as attenuation-corrected images. With the exception of certain areas of special artifacts (e.g., body surface), most tumors can be evaluated semiquantitatively on uncorrected images with an accuracy similar to that of attenuation-corrected images.

ACKNOWLEDGMENTS

We thank the staff of the Cyclotron Radioisotope Center and the Institute of Development, Aging and Cancer, Tohoku University, particularly Mr. Watanuki and Mr. Miyake, for their PET operation and excellent technical assistance. This work was supported by Grants-in-Aid Nos. 06454320 and 09470195 for Cancer Research from the Ministry of Education, Science, Sports and Culture, Japan.

REFERENCES

1. Fischmann AJ, Alpert NM. FDG PET in oncology: there's more to it than looking at pictures. *J Nucl Med* 1993;34:6–11.
2. Dichiro G, Brooks RA. PET quantitation: blessing and curse. *J Nucl Med* 1988;29: 1603–1605.
3. Engel H, Steinert H, Buck A, Berthold T, Boni RAH, Schulthess GKV. Whole body PET: physiological and artifactual fluorodeoxyglucose accumulations. *J Nucl Med* 1996;37:441–446.
4. Lowe VJ, Hoffman JM, DeLoong DM, Patz EF, Coleman RE. Semiquantitative and visual analysis of FDG PET images in pulmonary abnormalities. *J Nucl Med* 1994;35:1771–1776.
5. Bury T, Dowlati A, Paulus P, Hustinx R, Radermecker M, Rigo P. Staging of non small cell lung cancer by whole body FDG positron emission tromography. *Eur J Nucl Med* 1996;23:204–206.
6. Culbert PA, Adam MJ, Hurtado ET, et al. Automated synthesis [^{18}F]FDG using tetrabutylammonium bicarbonate. *Appl Radiat Isot* 1995;46:887–891.
7. Carson RE, Daube-Witherspoon ME, Green MV. A method for postinjection PET transmission measurements with a rotating source. *J Nucl Med* 1988;29:1558–1567.
8. Kubota K, Matsuzawa T, Ito M, et al. Lung tumor imaging by positron emission tomography using ^{11}C L-methiothinine. *J Nucl Med* 1985;26:37–42.
9. Links JM. Visual interpretation. In: Wagner HN, Szabo Z, Buchanan JW, eds. *Principal of nuclear medicine*, 2nd ed. Philadelphia: W.B. Saunders; 1995:391.
10. Lowe VJ, Duhaylongsod FG, Patz EF, et al. Pulmonary abnormalities and PET data analysis. A retrospective study. *Radiology* 1997;202:435–439.

A Preliminary Cell Kinetics Model of Thrombocytopenia After Radioimmunotherapy

Sui Shen, Gerald L. DeNardo, Troyce D. Jones, Richard B. Wilder, Robert T. O'Donnell and Sally J. DeNardo

Radiodiagnosis and Therapy Section, Division of Hematology/Oncology, and Radiation Oncology, University of California Davis, Cancer Center, Sacramento, California; Chemical and Biological Physics Section, Oak Ridge National Laboratory, Oak Ridge, Tennessee; and Veteran's Administration Northern California Health Care System, Martinez, California

Thrombocytopenia is often the dose-limiting toxicity for radionuclide therapy. Prediction of platelet counts after therapy is important for treatment planning. Simple prediction methods based on linear correlation between radiation dose and blood count nadir have been insufficient because they have not considered time, because of the complicated hierarchical structure of the hematopoietic system in which platelets are not directly injured by low dose rate radiation and because of changing radiation dose rates to marrow with time. This study addresses these problems using a cell kinetics model. **Methods:** The model consists of compartments for progenitor cells, megakaryocytes, platelets and stromal cells. A linear quadratic formula was used for progenitor cell survival. Stromal cells were described by a model based on a maximum likelihood estimate for cellular damage, repair and proliferation. Reported values for murine cellular turnover rates and radiosensitivity of progenitor cells were used in the model calculations. Experimental mice received 4 Gy of external beam radiation for tumor implantation and 12.4–23.3 MBq ^{67}Cu-2-iminothiolane-BAT-Lym-1 (BAT = 6-[p-(bromoacetamido) benzyl]−1,4,8,11-tetra-azacyclotetradecane-N,N′,N″,N‴-tetraacetic acid) 19–30 days later. Blood counts were measured three times each week. **Results:** The model predicted the severity of thrombocytopenia, and the time of the nadir corresponded to measured values in mice. For a dose of 14.2 MBq ^{67}Cu-2-iminothiolane-BAT-Lym-1 that induced a platelet nadir of 20% of baseline (Grade II), the model predicted that at least 20 days were needed before a second 14.2-MBq injection if a subsequent nadir of <10% of baseline (Grade IV) was to be avoided. **Conclusion:** The nadir and duration of thrombocytopenia predicted by the model were similar to those observed in the mice. Predicted information could be useful for planning the dose and timing of fractionated radionuclide therapy. This model provides a stepping stone for future development of a predictive model for patients.

Key Words: radionuclide therapy; radioimmunotherapy; marrow cell kinetics; radiation dosimetry; thrombocytopenia

J Nucl Med 1998; 39:1223–1229

Radiation-induced myelotoxicity is often dose-limiting in radionuclide therapy that does not include bone marrow reconstitution. The ability to predict peripheral blood counts after

Received Jun. 9, 1997; revision accepted Oct. 15, 1997.

For correspondence or reprints contact: Sui Shen, PhD, Radiodiagnosis and Therapy Section, 1508 Alhambra Boulevard, Room 214, Sacramento, CA 95816.

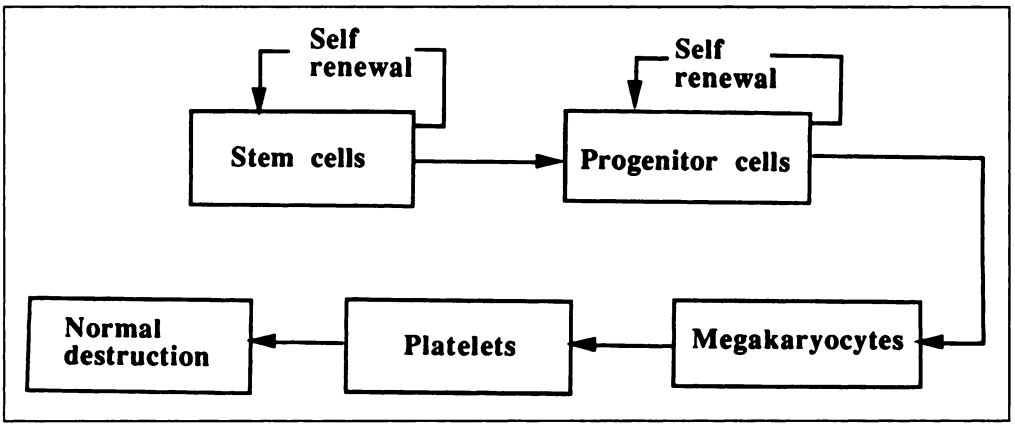

FIGURE 1. Schematic of thrombopoiesis. In steady state, normal platelet destruction is balanced by platelet production.

radionuclide therapy is important for treatment planning using radiation dosimetry. Investigations to date have not provided good predictions of peripheral blood counts based on the radiation dose delivered to bone marrow by radioimmunotherapy (RIT) (*1–5*). Difficulties in predicting the decrease in blood counts in response to radiation emitted by radiolabeled antibodies include a heterogeneous patient population previously treated with different types and doses of chemotherapy and radiotherapy (*1–5*), regional and microscopic nonuniform distribution of radioactivity in the marrow (*6*), the complicated hierarchical structure of the hematopoietic system in which platelets are indirectly injured by low dose rate radiation from RIT (*7*) and changing radiation dose rates to marrow with time.

The purpose of this study was to develop a simple cell kinetics model to address the hierarchical structure of the hematopoietic system and the time-varying radiation dose rate. A compartmental model was proposed to simulate the hierarchical structure of the hematopoietic system for cell proliferation. A linear quadratic formula was used for survival of progenitor cell. Platelet counts were the paradigm in the present analysis because thrombocytopenia is the major dose-limiting toxicity of RIT. Platelet counts predicted by the model were compared with those measured in mice treated with RIT.

MATERIALS AND METHODS

Mouse Model

Athymic *nu/nu* mice (Harlan Sprague-Dawley, Frederick, MD) received a single whole-body dose of 4 Gy by external beam irradiation to inhibit rejection of subsequently implanted human lymphoma (Raji) xenografts. Three days later, human Raji Burkitt's lymphoma cells were implanted. Sixteen to 27 days after implantation, groups of 8–13 mice received an intravenous injection of 12.4, 14.8, 18.5, 20.9 or 23.3 MBq ^{67}Cu-2-iminothiolane (2IT)-BAT-Lym-1 radiopharmaceutical (*8*). The radiopharmaceutical was prepared by conjugating the bifunctional chelate 6-[p-(bromoacetamido)benzyl]-1,4,8,11-tetra-azacyclotetradecane-N,N′,N″,N‴-tetraacetic acid (BAT) to murine antilymphoma IgG2a antibody, Lym-1, through 2IT. Blood samples were collected from mice within a dose group and were pooled. The pooled samples were diluted 1:100 in 1% (w/v) ammonium oxalate, and platelets were counted using a hemocytometer and light microscopy at a magnification of ×450. Body and blood activity were measured daily after dose administration (*8*).

Twelve mice received 18.5 MBq ^{67}Cu-2IT-BAT-Lym-1 and were dissected 5 min, 24 hr and 120 hr later to obtain femurs. The marrow (including blood in the marrow) in the femur was extracted using tissue solvent; marrow mass was determined by subtracting dry bone mass from that of femur. The ^{67}Cu concentration in the marrow (including blood in the marrow) was determined using a well counter.

Cell Survival for Time-Varying Radiation Dose Rate

The linear quadratic formula has been widely used to describe the single-dose (D) response curve for mammalian cells. In the absence of proliferation, the fraction of surviving cells (N/N_0) after irradiation is (*7,9,10*):

$$\ln\left(\frac{N}{N_0}\right) = -\alpha D - \beta D^2, \qquad \text{Eq. 1}$$

where N is the number of surviving cells, N_0 is the initial cell population, α is the coefficient of nonrepairable damage per Gy and β is the coefficient of repairable damage per Gy^2.

The radiation dose rate, r(t), at time t after injection of radiolabeled antibodies changes as a result of physical decay and biological clearance of the radionuclide in tissue. The cumulative radiation dose, D(t), at time t is:

$$D(t) = \int_0^t r(\tau)\, d\tau. \qquad \text{Eq. 2}$$

Taking the derivative of Equation 1, the differential equation governing the target cell population as a function of time is:

$$\frac{dN(t)}{dt} = -[\alpha r(t) + 2\beta D(t) r(t)] N(t). \qquad \text{Eq. 3}$$

Cell Kinetics Model for Platelets

Although cellular function and homeostasis are extremely complex, the hematopoietic system can be simplified using a qualitative model consisting of stem cells, progenitor cells, differentiated cells (megakaryocytes) and functional peripheral blood cells (platelets) (Fig. 1) (*11–16*). Because the pluripotential stem cells divide only once every 3–4 yr, their impact on cell production during the period of RIT is negligible (*15*). Therefore, the stem cell compartment was excluded in this model.

For the low dose rate irradiation characteristic of RIT (*7*), the radiation damage was suffered primarily by the radiosensitive progenitor cells, as demonstrated by spleen colony-forming unit (CFU-S) assays (*15*). Low dose rate radiation damage to platelets and megakaryocytes is relatively insignificant (*14*). Incorporating Equation 3, the differential equations describing the population of progenitor cells, megakaryocytes and platelets are (lower part of Fig. 2):

$$\frac{dN(t)_{prog}}{dt} = -[\alpha r(t) + 2\beta D(t) r(t)] N(t)_{prog} + \lambda(t)_{prog\to prog} F(t)_{stro\to prog} N(t)_{prog} - \lambda_{prog\to Mega} N(t)_{prog}; \qquad \text{Eq. 4}$$

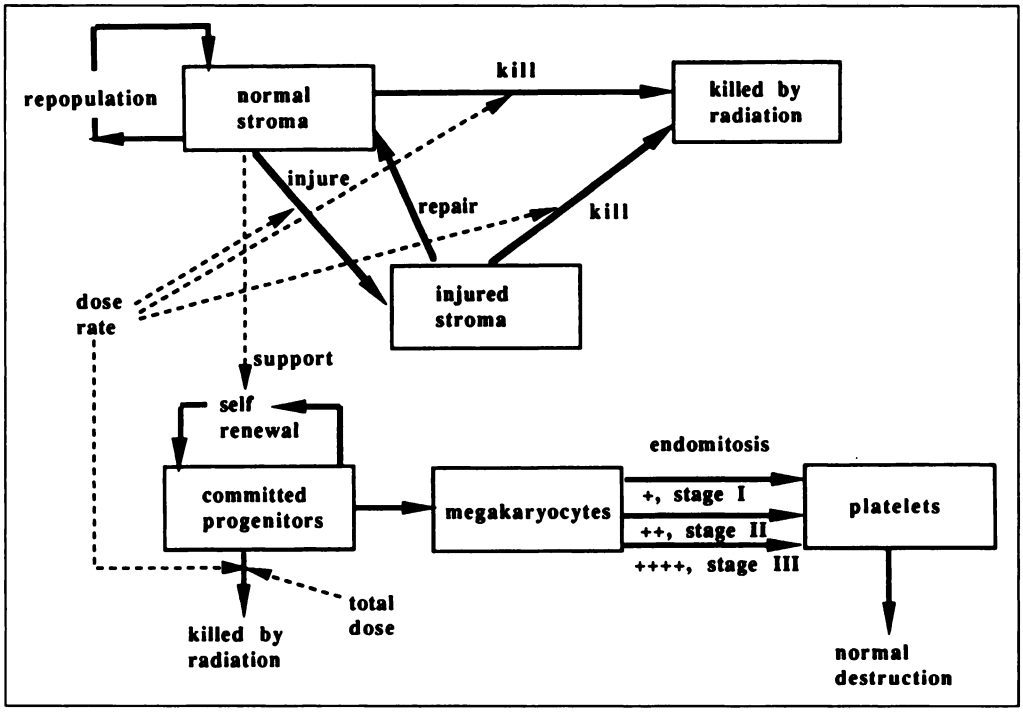

FIGURE 2. Compartmental model describing simplified, central rules governing thrombopoiesis and effects of irradiation. Solid arrows represent cell flow from one compartment to another. Dashed arrows are factors affecting rate of cell flow. Both linear and quadratic terms in linear-quadratic equation represented cell flow out of progenitor compartment and were labeled as kill by radiation.

$$\frac{dN(t)_{Mega}}{dt} = \lambda_{prog\rightarrow Mega}\, N(t)_{prog} - \lambda_{Mega\rightarrow plat}\,(2^3 - 1)A\, N(t)_{Mega}; \quad \text{Eq. 5}$$

$$\frac{dN(t)_{plat}}{dt} = \lambda_{Mega\rightarrow plat}\,(2^3 - 1)A\, N(t)_{Mega} - \lambda_{plat\rightarrow dest}\, N(t)_{plat}, \quad \text{Eq. 6}$$

where $N(t)_{prog}$, $N(t)_{Mega}$ and $N(t)_{plat}$ are cell populations at time t for progenitor cells, megakaryocytes and platelets, respectively. The $\lambda(t)_{prog\rightarrow prog}$, $\lambda_{prog\rightarrow]Mega}$, $\lambda_{Mega\rightarrow plat}$ and $\lambda_{plat\rightarrow dest}$ are rate constants for progenitor cell to progenitor cell (self-renewal) at time t, progenitor cells to megakaryocytes, megakaryocytes to platelets and platelets to normal destruction, respectively. An amplification factor of $(2^3 - 1)A$ is used as megakaryocyte polyploid increases 7 times (or $2^3 - 1$) through three stages of endomitosis, assuming an A number of platelets were released from megakaryocytes before endomitosis (*16*). $F(t)_{stro\rightarrow prog}$ is a regulation factor reflecting the condition of the supporting stromal microenvironment.

Before irradiation, the hematopoietic system was assumed to be in steady state as platelet destruction was balanced by platelet production (*16*). This simplification leads to equilibrium at time zero:

$$\lambda(0)_{prog\rightarrow prog}\, F(0)_{stra\rightarrow prog} N(0)_{prog} = \lambda_{prog\rightarrow Mega}\, N(0)_{prog} = \lambda_{Mega\rightarrow plat}\,(2^3 - 1)A\, N(0)_{Mega} = \lambda_{plat\rightarrow dest}\, N(0)_{plat}. \quad \text{Eq. 7}$$

Stromal Microenvironment

Progenitor cells are supported and grow in a stromal microenvironment. Because stromal cells are not of hematologic origin, stromal cells were modeled independently. A simple stromal model was derived from the report of Jones et al. (*17,18*) for the low dose rate radiation of RIT that varies with time (Fig. 2, upper). A three-compartment stromal model considered the processes of sublethal injury, repair of sublethal injury, "one-hit" killing, "two-hit" killing and proliferation. These processes can be simply described as:

$$\frac{dN(t)_{Snor}}{dt} = \lambda_{Snor\rightarrow Snor}\, N(t)_{Snor} - \lambda_{Snor\rightarrow Sinj}\, r(t)N(t)_{Snor} - \lambda_{Snor\rightarrow Skil}\, r(t)N(t)_{Snor} \quad \text{Eq. 8}$$

and

$$\frac{dN(t)_{Sinj}}{dt} = \lambda_{Snor\rightarrow Sinj} r(t)N(t)_{Snor} - \lambda_{Sinj\rightarrow Snor}\, N(t)_{Sinj} - \lambda_{Sinj\rightarrow Skil}\, N(t)_{Sinj}, \quad \text{Eq. 9}$$

where $N(t)_{Snor}$ and $N(t)_{Sinj}$ represent the number of normal and injured stromal cells at time t; $\lambda_{Snor\rightarrow Snor}$, $\lambda_{Snor\rightarrow Sinj}$, $\lambda_{Snor\rightarrow Skil}$, $\lambda_{Sinj\rightarrow Snor}$ and $\lambda_{Sinj\rightarrow Skil}$ are rate constants for proliferation, normal to sublethal injury, normal to one-hit killing, repair of sublethal injury and two-hit killing of stromal cells, respectively (*18*).

In this study, the main effect of the stromal microenvironment on hematopoiesis was simplified as a regulation factor for progenitor cell self-renewal. The factor $[F(t)_{stro\rightarrow prog}]$, which regulates the rate constant of progenitor cell self-renewal, was assumed to be proportional to the number of normal stromal cells at time t:

$$F(t)_{stro\rightarrow prog} = a\,\frac{N(t)_{Snor}}{N(0)_{Snor}} + b, \quad \text{Eq. 10}$$

where a and b are scaling constants, and $N(0)_{Snor}$ is the initial population of normal stromal cells.

Marrow Radiation Dose Rate from Copper-67-2IT-BAT-Lym-1

Body and marrow clearance were fitted with a monoexponential function. The effective half-life was 49.6 hr for whole body (*8*) and 59.7 hr for marrow (including blood in the marrow). The radiation dose to marrow was calculated by summating penetrating radiation from whole body and nonpenetrating radiation from marrow (including blood in the marrow). The absorbed fraction of photons in a 20-g mouse was obtained from MIRD data (*19*). The penetrating radiation dose rate, $r_{body}(t)$, to the marrow from the whole body was $0.0027\ \exp(-0.693t/2.07)$ Gy/day/MBq.

The range for 90% absorption, X_{90}, for 150-keV beta emissions is 0.56 mm (*20*). For a cylindrical marrow cavity of 1-mm diameter (*21*), an absorbed fraction of 65% was estimated for ^{67}Cu mean beta energy of 150 keV using MIRD data (*20*). The nonpenetrating radiation dose rate, $r_{marrow}(t)$, to marrow from marrow (including blood in the marrow) was $0.079\ \exp(-0.693t/2.49)$ Gy/day/MBq.

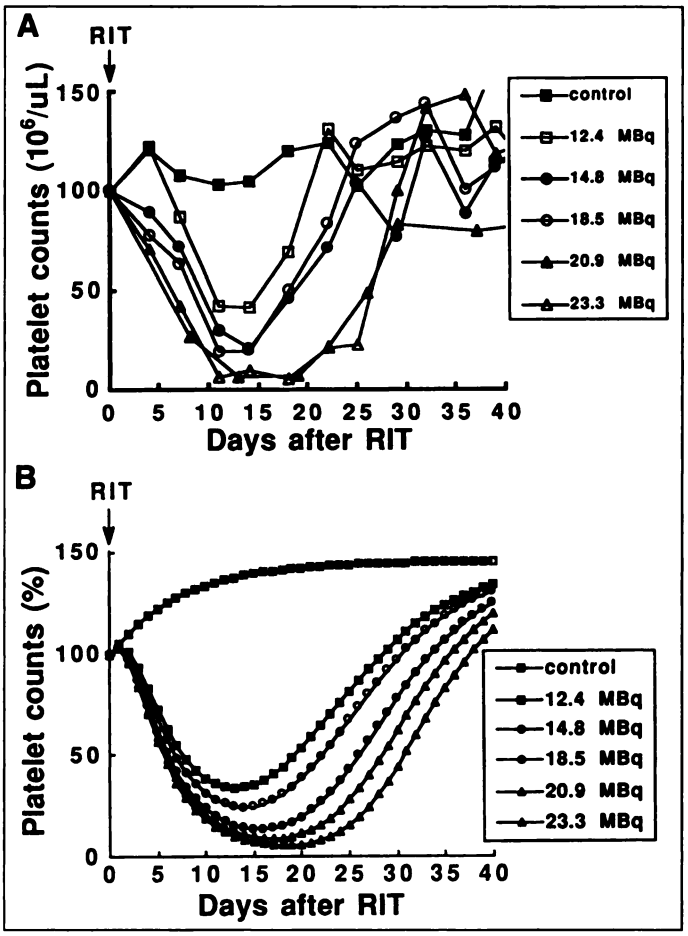

FIGURE 3. (A) Measured platelet counts in mice after no treatment (control) and treatment with ^{67}Cu-2IT-BAT-Lym-1. All counts were normalized to initial counts at beginning of RIT. All mice received 4 Gy whole-body external beam radiation 19 to 30 days before RIT for Raji cell implantation. (B) Mean time interval between external beam radiation and RIT of 25 days was assumed in model. All counts were normalized to initial counts at beginning of RIT (25 days after 4-Gy external beam). Predicted platelet counts after RIT were similar to those measured in experiments.

Computation

The numerical computation of the above differential equations was implemented using the software program STELLA (High Performance, Lyme, NH) on a Macintosh computer. A schematic representation of these differential equations is illustrated in Figure 2. The Euler numerical method was used (and was confirmed by the Runge–Kutta method) to solve the above differential equations with a time step of 0.01 day. Selection of initial parameters for the computation is described in the Appendix.

RESULTS

Groups of mice received 12.4–23.3 MBq ^{67}Cu-2IT-BAT-Lym-1 19 to 30 days after the external beam radiation needed for Raji cell implantation. The nadir of platelet counts was lower and occurred later (from 14 to 18 days) after injection of ^{67}Cu-2IT-BAT-Lym-1 as the ^{67}Cu dose increased from 12.4 to 23.3 MBq (Fig. 3A). The slight increase in platelet counts in the control and 12.4 MBq groups after the injection of ^{67}Cu-2IT-BAT-Lym-1 was due to platelet recovery from the external beam radiation.

In the cell kinetics model calculation, the values used for ^{67}Cu dose level and time interval between external beam radiation and RIT corresponded to the experimental conditions. Using an average time interval of 25 days, the predicted platelet counts as a function of time after RIT were similar to measured platelet counts in the mice (Fig. 3B). Likewise, the predicted platelet nadirs were in good agreement with the measured values (Table 1).

The model predicted that the time interval between multiple therapies had a substantial impact on platelet counts. The model-predicted progenitor, stromal and platelet counts are illustrated for the 12.4- or 23.3-MBq dose levels and time intervals of 19 and 30 days (Fig. 4). The predicted platelet counts recovered to 38% of the initial counts at 19 days and to 84% at 30 days after 4 Gy of external beam radiation.

In the model calculation, a single dose of 14.2 MBq ^{67}Cu-2IT-BAT-Lym-1 resulted in a nadir that was 20% of the baseline (Fig. 5). For a mean baseline platelet count of 250,000/μl in humans (*22*), National Cancer Institute toxicity Grades I (75,000–100,000/μl), II (50,000–75,000/μl) and III (25,000–50,000/μl) correspond to nadirs of 30%–40%, 20%–30% and 10%–20%, respectively. The model predicted that at least 20 days were needed before a second 14.2-MBq injection if a subsequent nadir of $<$10% of baseline (Grade IV) was to be avoided in mice. On the other hand, if the second dose was delayed until 30 days after the first dose (counts recovered to 69%), then the subsequent nadir predicted by the model would be 17% and the duration of Grade III toxicity would be shortened to 6 days. The predicted platelet counts recover to 68% at 30 days after the second dose, so that, in theory, one could deliver fractionated therapy at this interval.

DISCUSSION

Although myelotoxicity after RIT has received much attention (*1–6*), current prediction methods based on linear correlation between marrow radiation dose and blood count nadir have been insufficient because they have not considered time and have not allowed accurate prediction of peripheral blood counts

TABLE 1
Mouse Platelet Counts After Radioimmunotherapy (RIT) with Copper-67-2IT-BAT-Lym-1*

	Experimental		Model-predicted	
Injected ^{67}Cu (MBq)	Time to nadir after RIT (days)	Nadir relative to initial RIT (% of baseline)	Time to nadir after RIT (days)	Nadir relative to initial RIT (% of baseline counts)
12.4	14	41	13	34
14.8	14	21	14	24
18.5	13	19	15	14
20.9	16	6	17	9
23.3	18	5	18	6

*Averaged nadir platelet counts were expressed relative to the initial counts at the beginning of RIT. Because all mice received 4 Gy of external beam radiation 19 to 30 days before RIT, a mean time interval between external beam radiation and RIT of 25 days was assumed in the model calculation.

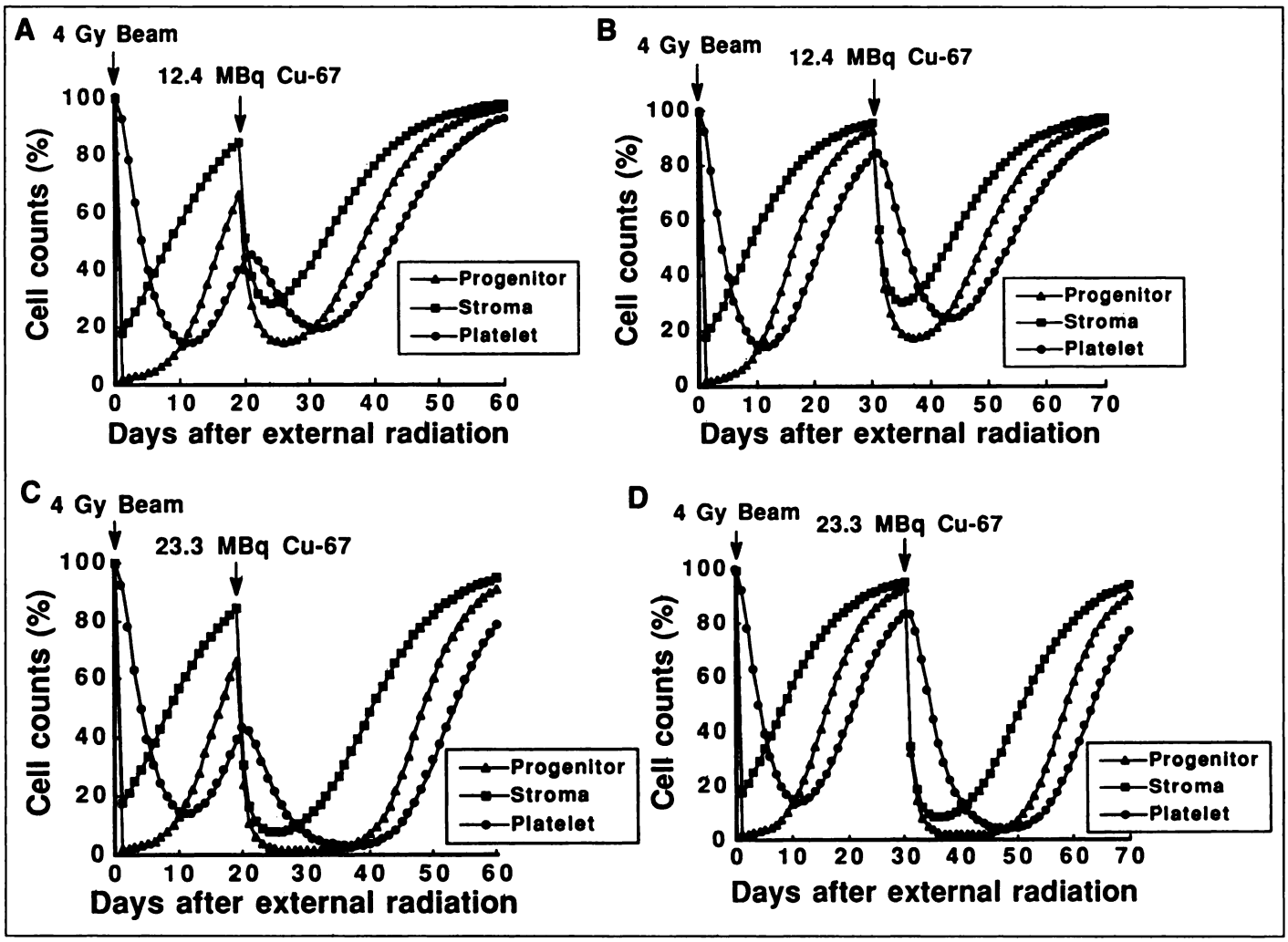

FIGURE 4. Predicted hematopoietic cell population after 4 Gy whole-body external beam radiation and subsequent ^{67}Cu-2IT-BAT-Lym-1. Injected radioactivity of ^{67}Cu and time interval between external beam radiation and RIT were (A) 12.4 MBq and 19 days (B) 12.4 MBq and 30 days (C) 23.3 MBq and 19 days; and (D) 23.3 MBq and 30 days.

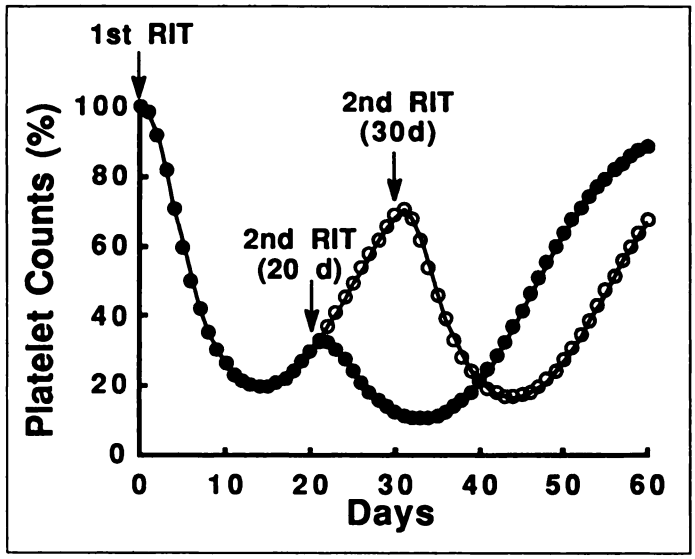

FIGURE 5. Timing for RIT dose that induces a 20% nadir predicted by model. If second dose is delayed until 30 days after first dose (platelet counts recover to 69%), then duration of Grade III toxicity will be shortened to 6 days, and platelet counts will recover to 68% at 30 days after second dose, so, in theory, repetitive doses could be delivered at this interval.

based on the radiation dose delivered to the bone marrow. These investigations have faced difficulties, including a heterogeneous patient population previously treated with different types and doses of chemotherapy and radiotherapy (*1–5*), regional and microscopic nonuniform distribution of radioactivity in the marrow (*6*), the complicated hierarchical structure of the hematopoietic system in which platelets are indirectly injured by low dose rate radiation from RIT (*7*) and changing radiation dose rates to marrow with time.

This study focused on the hierarchical structure of the hematopoietic system and the time-varying irradiation to marrow. Platelets are not directly damaged by the low dose rate irradiation from RIT. Platelet counts depend on production from progenitor cells and normal daily destruction of platelets (Fig. 2). The radiation dose rate delivered to the marrow changes as a function of physical decay and biological clearance of the radionuclide. This study addressed the problem of this hierarchical structure using a cell kinetics model and the problem of time-dependent irradiation using a linear-quadratic formula for survival of progenitor cells.

The ranges of ^{67}Cu beta emissions are small relative to the dimension of marrow cavities in patients. This results in nonuniform radiation to patient marrow. In the mouse model, the dimensions of marrow are within the beta emission range of ^{67}Cu, and the marrow is free of malignant cells, so that the problem of nonuniform radiation is negligible. The issue of

variable bone marrow reserve due to previous chemotherapy was avoided in this mouse model. However, the mouse model did predict the platelet decrease after ^{67}Cu radiation after external beam radiation, a somewhat comparable situation to that of patients who had received prior radiation therapy. Although the issues of prior chemotherapy and nonuniform radiation to marrow are not directly addressed in the present cell kinetics model, they are important issues that may affect prediction of the dose response in patients. However, this study constitutes a stepping stone toward a more comprehensive solution by addressing the hierarchical structure of the hematopoietic system and time-dependent irradiation. Further investigations are worthwhile for different mouse models and various therapeutic radionuclides.

Jones et al. (*17,18*) modeled kinetics of "critical" stromal cells implicitly for damage, repair, killing and proliferation using mortality data. Their stromal and stem cell model was not directly linked to differentiation and proliferation. A different approach was used in this study. Progenitor cells, megakaryocytes and platelets are linked directly to predict peripheral blood counts.

Because cell functions in the hematopoietic system are extremely complex, an exact cell kinetics model is difficult to construct. The present approach to this complex problem involved the stripping away of second-order effects that are difficult to assess so that more essential effects could be treated simply. For example, direct radiation insults to megakaryocytes were neglected because megakaryocytes are radioresistant to sublethal irradiation (*14*). The changes in postmitotic megakaryocyte maturation and the rate of platelet release were assumed to be relatively small compared to changes in progenitor self renewal for maintaining homeostasis of the progenitor cell pool because progenitor cells were directly depleted by low dose rate radiation.

There is a complex humoral feedback through cytokines for hematopoietic homeostasis, and the daily platelet count oscillates above and below homeostasis. However, the process can be effectively averaged out over the period of observation because platelet destruction is exactly balanced by platelet production in the steady state (*16*). Because of this simplification, the exact ratio of progenitor cells that self renew and differentiate becomes insignificant in the present model calculation. Therefore, the choices of these parameters are not critical for the present model calculation.

The α value for progenitor cell and absorbed fraction for ^{67}Cu energy in mouse marrow are critical for the model calculation. For example, a change in the α value from 0.65 to 0.81 Gy^{-1} equals a change in injected radioactivity from 18.5 to 14.8 MBq. In this study, the reported radiosensitivity of CFU-S in response to electron energies similar to the beta energies emitted by ^{67}Cu was used (*23*). An absorbed fraction of 0.65 was estimated based on MIRD data (*20*) assuming a cylindrical marrow cavity of 1 mm diameter (*21*). This absorbed fraction value is close to the value reported for ^{131}I (*24*). The results of this study illustrated a strong association between the predicted and measured platelet counts using the defined methods and parameters (Table 1). However, further investigation is needed of the radiosensitivity of progenitor cells to various therapeutic radionuclides, such as the response of granulocyte-macrophage colony-forming cells to ^{90}Y (*25*).

The dominant radiation to the marrow is nonpenetrating from ^{67}Cu in marrow (including blood in the marrow). Although the marrow uptake of radionuclide is not routinely measured in patients (*26,27*), the marrow radioactivity was predominantly contributed by radioactivity in the blood in marrow (*8*). The present model still provided a relatively good prediction of platelet counts when blood was considered as the only nonpenetrating source. For example, assuming 25 days between RIT and external radiation, the model predicted a nadir of 23% or 12% (of initial RIT counts) in response to injection of 18.5 or 23.3 MBq ^{67}Cu-2IT-BAD-Lym-1.

Although the predicted platelet counts using the cell kinetics model agreed with the measured counts in mice after RIT, the model cannot be simply applied to patients. Mouse bone marrow consists of 100% red marrow. Red marrow content in man decreases with age and is slowly replaced by yellow marrow. Many model parameters for humans will be different from those for mice. For example, the life span of human platelets is longer than that in mice. Although this model can be used as a starting point, additional research and, possibly, modifications of the model are needed before efforts to predict platelet counts after RIT in patients.

CONCLUSION

Although the hematopoietic system is complex and simplifications were used, this cell kinetics model predicted platelet counts any time after RIT. Predicted information will be helpful in planning the radioactive dose and timing for RIT. This model provides a stepping stone for future application to predict myelotoxicity in patients after RIT. This compartmental model can be implemented easily with computer software.

ACKNOWLEDGMENTS

This work was supported by a grant from the National Cancer Institute (USPHS CA47829).

APPENDIX: INITIAL PARAMETER VALUES

Because only the relative number (percentage) of surviving cells was required in this model, 100 was chosen as the initial value (baseline), $N(0)_{plat}$, for simplicity. Because the life span of platelets in mice is reported to be ~5 days (*14*), the corresponding rate constant, $\lambda_{plat\rightarrow dest}$, is 0.693/2.5 day^{-1}. As estimated from DNA labeling in rats, the total megakaryocyte maturation time is ~60 hr, and seven mature megakaryocytes are generated to release platelets (*16*). The effective rate constant, $\lambda_{Mega\rightarrow plat}$, is 0.693/0.9 day^{-1}. The initial megakaryocyte population was derived using Equation 7, $(2^3 - 1)A\ N(0)_{Mega} = (0.693/2.5)/(0.693/0.9) \times 100 = 36$.

From published studies on cycle times for hematopoietic progenitor cells, there is typically a twofold shortening of the cell cycle under a strong stimulus for proliferation that suggests a variable doubling time ranging from 12 to 24 hr (*17*). Based on these estimates, an initial value of 0.693/1 day^{-1} was used for $\lambda(0)_{prog\rightarrow prog}$. The value $\lambda(t)_{prog\rightarrow prog}$ increased to 0.693/0.5 day^{-1} as progenitor cells were depleted. Therefore, the rate constant for progenitor cell renewal was:

$$\lambda(t)_{prog\rightarrow prog} = \frac{0.693}{0.5 + 0.5N(t)_{prog}/N(0)_{prog}}\ day^{-1}, \quad \text{Eq. 1A}$$

where $N(0)_{prog}$ was the initial number of progenitor cells. At each progenitor cell doubling, one cell was assumed to enter the megakaryocyte compartment, and one progenitor cell was assumed to self renew. Therefore, $\lambda_{Mega\rightarrow prog} = \lambda(0)_{prog\rightarrow prog} = 0.693/1\ day^{-1}$.

The probability of bone marrow recovery in the mice is high if the population of stromal cells is above a critical point of 0.2% (*18*). Based on this estimate, we assumed that even at a maximum rate of 0.693/0.5 day^{-1} for $\lambda(t)_{prog\rightarrow prog}$, $F(t)_{stra\rightarrow prog}\lambda(t)_{prog\rightarrow prog}$ was less than $\lambda_{Mega\rightarrow prog}$ when stromal cells were below 0.2%. The scaling constants in Equation 10 (500/998 for a and 498/998 for b) were determined based on $F(0)_{stra\rightarrow prog} = 1$ and $F(t)_{stra\rightarrow prog}\lambda(t)_{prog\rightarrow prog} = \lambda_{Mega\rightarrow prog}$ at the critical point.

The initial progenitor cell population, $N(0)_{prog}$, was:

$$N(0)_{prog} = \frac{\lambda_{plat \rightarrow dest}\, N(0)_{plat}}{F(0)_{stra \rightarrow prog}\, \lambda(0)_{prog \rightarrow prog}} = \frac{0.693/2.5 \times 100}{1 \times 0.693/1} = 40, \quad \text{Eq. 2A}$$

using Equation 7.

The radiosensitivity of mouse progenitor cells to ^{67}Cu (mean beta energy = 150 keV) has not been reported in the literature. An α value of 0.65 Gy^{-1} was selected based on the reported radiosensitivity of 0.64 to 0.68 Gy^{-1} to 100 to 300 keV electrons for mouse CFU-S (*23*). The α and β values for mouse CFU-S irradiated with ^{60}Co photons were used to approximate the value for 4 MV of external beam radiation (α of 0.7 Gy^{-1}, β of 0.07 Gy^{-2} in vivo) (*11*).

The published numerical constants for a stromal cell model were used in Equations 8 and 9. From reported sets of constants for 100- and 250-kVp x-rays, ^{137}Cs and ^{60}Co photons (*18*), constants for 100-kVp x-rays were selected to approximate those for beta emissions from ^{67}Cu. Constants for ^{60}Co photons were selected to approximate those for 4 MV of external beam radiation.

REFERENCES

1. DeNardo GL, DeNardo SJ, Macey DJ, Shen S, Kroger LA. Overview of radiation myelotoxicity secondary to radioimmunotherapy using I-131-Lym-1 as a model. *Cancer* 1994;73(suppl):1038–1048.
2. Wilder RB, Fowler JF, DeNardo GL, Shen S, Wessels BW, DeNardo SJ. Use of the linear-quadratic model to compare doses delivered to the bone marrow by fractionated I-131-Lym-1. *Antibody Immunoconj Radiopharm* 1995;8:227–239.
3. Juweid M, Behr T, Sharkey RM, Dunn R, Rubin AD, Goldenberg DM. Factors affecting the relationship between the red marrow dose and myelotoxicity in patients receiving radioimmunotherapy with I-131-labeled anti-CEA monoclonal antibodies [Abstract]. *J Nucl Med* 1996;37:43p.
4. Eary JF, Krohn KA, Press OW, Fisher D, Bernstein ID. Radioimmunotherapy treatment planing based on radiation absorbed dose or patient size [Abstract]. *J Nucl Med* 1996;37:43p.
5. Sgouros G, Divgi CR, Scott AM, Williams J, Larson SM. Hematologic toxicity in radioimmunotherapy: an evaluation of different predictive measures [Abstract]. *J Nucl Med* 1996;5:43p.
6. Sgouros G, Jureidini IM, Scott AM, Graham MC, Larson SM, Scheinberg DA. Bone marrow dosimetry: regional variability of marrow-localizing antibody. *J Nucl Med* 1996;37:695–698.
7. Fowler JF. Radiobiological aspects of low dose rates in radioimmunotherapy. *Int J Radiat Oncol Biol Phys* 1990;18:1261–1269.
8. DeNardo GL, Kukis DL, Shen S, et al. Efficacy and toxicity of Cu-67-2IT-BAT-Lym-1 radioimmunoconjugate in mice implanted with human Burkitt's lymphoma (Raji). *Clin Cancer Res* 1997;3:71–79.
9. Dale RG. The application of the linear-quadratic dose-effect equation to fractionated and protracted radiotherapy. *Br J Radiol* 1985;58:515–528.
10. O'Donoghue JA. The impact of tumor cell proliferation in radioimmunotherapy. *Cancer* 1994;73:974–980.
11. Hendry JH, Lord BI. The analysis of the early and late response to cytotoxic insults in the haemopoietic cell hierarchy. In: Potten CS, Hendry JH, eds. *Cytotoxic insult to tissue*. Edinburgh: Churchill-Livingstone; 1983:1–66.
12. Testa NG, Hendry JH, Molineux G. Long-term bone marrow damage in experimental systems and in patients after radiation or chemotherapy. *Anticancer Res* 1985;5:101–110.
13. Schofield R. Assessment of cytotoxic injury to bone marrow. *Br J Cancer* 1986; 53(suppl 7):115–125.
14. Ebbe S. Origin, production and life-span of blood platelets. In: Johnson SA, ed. *The circulating platelet*. New York: Academic Press; 1971:19–43.
15. Ratajczak MZ, Gewirtz AM. The biology of hematopoietic stem cells. *Semin Oncol* 1995;22:210–217.
16. Bithell TC. Platelets and megakaryocytes. In: Lee GR, Bithell TC, Foerster J, Athens JW, Lukens JN, eds. *Wintrobe's clinical hematology*, 9th ed. Philadelphia and London: Lea & Febiger; 1993:511–530.
17. Jones TD, Morris MD, Young RW. A mathematical model for radiation-induced myelopoiesis. *Radiat Res* 1991;128:258–266.
18. Jones TD, Morris MD, Young RW. Mathematical models of marrow cell kinetics: differential effects of protracted irradiations on stromal and stem cells in mice. *Int J Radiat Oncol Biol Phys* 1993;26:817–830.
19. Ellett WH, Humes RM. *Absorbed fractions for small volumes containing photon-emitting radioactivity*. MIRD pamphlet no. 8. New York: Society of Nuclear Medicine; 1971.
20. Berger MJ. *Distribution of absorbed dose around point sources of electrons and beta particles in water and other media*. MIRD pamphlet no. 7. New York: Society of Nuclear Medicine; 1971.
21. Hui ED, Fisher DR, Kuhn JA, Williams LE, Nourigat C, Badger CC, Beatty BG, Beatty JD. A mouse model for calculating cross-organ beta doses from yttrium-90-labeled immunoconjugates. *Cancer* 1994;73(suppl):951–957.
22. Report of the task group on reference man. In: Snyder WS, Cook MJ, Nasset ES, et al. *International Commission on Radiological Protection*, no. 23. Oxford: Pergamon Press; 1974:38.
23. Watt DE. Track structure data for ionizing radiation in liquid water. In: *University report* BIOPHYS 10. St. Andrews, Scotland: University of St. Andrews; 1989.
24. Muthuswamy MS, Roberson PL, Buchsbaum. A mouse bone marrow dosimetry model [Abstract]. *Med Phys* 1996;23:1090.
25. Goddu SM, Howell RW, Rao DV. Biological dosimetry of bone marrow for incorporated Y-90 [Abstract]. *J Nucl Med* 1997;38:118p.
26. Siegel JA, Wessels BW, Waston EE, et al. Bone marrow dosimetry and toxicity for radioimmunotherapy. *Antib Immunoconjug Radiopharm* 1990;3:213–233.
27. Shen S, DeNardo GL, DeNardo SJ, et al. Dosimetric evaluation for radioimmunotherapy of Cu-64-2IT-BAT-Lym-1 in Cu-67-2IT-BAT-Lym-1 for radioimmunotherapy. *J Nucl Med* 1996;37:146–150.